

The evolution of iron-core white dwarfs

J. A. Panei,[★] L. G. Althaus[†] and O. G. Benvenuto[‡]

Facultad de Ciencias Astronómicas y Geofísicas, Paseo del Bosque S/N, (1900) La Plata, Argentina

Accepted 1999 September 30. Received 1999 September 20; in original form 1998 November 16

ABSTRACT

Recent measurements by *Hipparcos* present observational evidence supporting the existence of some white dwarf (WD) stars with iron-rich core composition. In connection with this, the present paper is aimed at exploring the structure and evolution of iron-core WDs by means of a detailed and updated evolutionary code. In particular, we examined the evolution of the central conditions, neutrino luminosity, surface gravity, crystallization, internal luminosity profile and ages. We find that the evolution of iron-rich WDs is markedly different from that of their carbon–oxygen counterparts. In particular, cooling is strongly accelerated (up to a factor of 5 for models with pure iron composition) as compared with the standard case. Thus, if iron WDs were very numerous, some of them would have had time enough to evolve at lower luminosities than that corresponding to the fall-off in the observed WD luminosity function.

Key words: stars: evolution – stars: interiors – white dwarfs.

1 INTRODUCTION

Although the theory of electron degeneracy is widely accepted amongst the astronomical community, up to very recently its observational basis was not solid enough. Obviously, the most useful objects for testing such a theory are white dwarf (WD) stars. It is known that the structure of WDs is almost completely dominated by electron degeneracy. The theory of WD stars predicts a mass–radius relation (Chandrasekhar 1939) that can be compared with observational tests. Because of the great importance of the theory of electron degeneracy in several astrophysical circumstances, great effort has been devoted to improving our knowledge of the mass–radius relation for WD stars.

In this sense, recent observations carried out by the astrometric satellite *Hipparcos* have allowed Provencal et al. (1998) to substantially improve the mass and radius determination for 20 WDs, either single or members of binary systems. From very accurate parallaxes, these authors determined precise mass and radius values, without invoking mass–radius relations, thus making these WDs excellent targets for testing stellar degeneracy directly. On the basis of these observations, Provencal et al.

suggest in particular that at least three objects of their WD sample appear to have an interior chemical composition consistent with iron. Indeed, GD 140, EG50 and Procyon B have stellar radii that, for their observed masses, are significantly smaller than those corresponding to a carbon–oxygen (CO) interior. Needless to say, such results, if correct, are clearly at odds with the standard theory of stellar evolution, which predicts a CO interior for intermediate mass WDs.

It is nevertheless worth noticing that the only proposal for a physical process able to account for the formation of iron WDs is, to our knowledge, by means of explosive ignition of electron-degenerate ONeMg cores (Isern, Canal & Labay 1991). In their calculations, Isern et al. (1991) find that, depending critically upon the ignition density and the velocity of the burning front, such an explosive ignition may lead to the formation of neutron stars, thermonuclear supernovae or iron WDs.

Interestingly enough, the implications of Provencal et al.’s results about the possible existence of a population of iron WDs coupled to the lack of modern theoretical studies about iron-core WDs in the literature, make it worthwhile to perform a detailed exploration of the structure and evolution of such objects. As a matter of fact, to our knowledge the only study of the evolution of iron WDs was performed long ago by Savedoff, Van Horn & Vila (1969); however, it was based on very simplified assumptions such as the neglect of convection, crystallization and electrostatic corrections to the equation of state. At first glance, one may think that the evolution of these objects could be markedly different from their CO counterparts. To place this suspicion on a more quantitative basis, we have carried out a comprehensive study of the properties of iron-core WDs with the emphasis placed on their evolution.

[★]Fellow of the Universidad Nacional de La Plata, Argentina. E-mail: panei@fcaglp.fcaglp.unlp.edu.ar.

[†]Member of the Carrera del Investigador Científico y Tecnológico, Consejo Nacional de Investigaciones Científicas y Técnicas (CONICET), Argentina. E-mail: althaus@fcaglp.fcaglp.unlp.edu.ar.

[‡]Member of the Carrera del Investigador Científico, Comisión de Investigaciones Científicas de la Provincia de Buenos Aires, Argentina. E-mail: obenvenuto@fcaglp.fcaglp.unlp.edu.ar.

The present paper is organized as follows: in Section 2 we briefly describe our evolutionary code. In Section 3 we summarize our main results. Finally, Section 4 is devoted to discussing the implications of our results and to making some concluding remarks.

2 THE EVOLUTIONARY CODE

The calculations we present below were performed with the same evolutionary code that we employed in our previous works on WDs, and we refer the reader to Althaus & Benvenuto (1997, 1998) for details about both the physical ingredients that we incorporated and the procedure that we followed to generate the initial models. In particular, the equation of state for the low-density regime is that of Saumon, Chabrier & Van Horn (1995) for hydrogen and helium plasmas, while the treatment for the high-density regime (solid and liquid phases) includes ionic contributions, Coulomb interactions, partially degenerate electrons, and electron exchange and Thomas–Fermi contributions at finite temperature. The harmonic phonon contribution is that of Chabrier (1993).

High-density conductive opacities and the various mechanisms of neutrino emission for different chemical compositions (^4He , ^{12}C , ^{16}O , ^{20}Ne , ^{24}Mg , ^{28}Si , ^{32}S , ^{40}Ca and ^{56}Fe) are taken from the works of Itoh and collaborators (see Althaus & Benvenuto 1997 for details). In addition to this, we include conductive opacities and Bremsstrahlung neutrinos for the crystalline lattice phase following Itoh et al. (1984a) and Itoh et al. (1984b; see also erratum), respectively. The latter becomes relevant for WD models with iron core, because, as it will be clear later, these models begin to develop a crystalline core at high stellar luminosities.

In Fig. 1 we show the conductive opacity at some selected temperature values for iron, and for 50 per cent carbon–50 per cent oxygen plasmas. The downward steps are due to the crystallization of the plasmas. Indeed, thermal conductivity in the crystalline phase becomes a factor 2–4 smaller near the melting temperature (see Itoh et al. 1984a; Itoh, Hayashi & Kohyama 1993 for details), which, as we shall see, will affect the rate of cooling of iron WD models.

With regard to neutrino emission rates, we have considered photo, pair, plasma and Bremsstrahlung neutrino contributions. The total emission rate is shown in Fig. 2 for the same cases as considered in Fig. 1. For a given temperature, the dominant neutrino emission process at low densities is photoneutrinos. At higher densities there is a bump in the emission rate owing to plasma neutrinos, whereas at higher densities Bremsstrahlung neutrinos take over. Clearly, at high densities, neutrino energy losses for iron plasmas become much more pronounced than for CO plasmas.

With respect to the energy transport by convection, we adopt the mixing length prescription usually employed in most WD studies. Finally, we consider the release of latent heat during crystallization in the same way as in Benvenuto & Althaus (1997).

3 EVOLUTIONARY RESULTS

In this section we shall describe the main results that we have found on the evolution of iron WDs. We have considered models with masses of $M/M_\odot = 0.50, 0.60, 0.70, 0.80, 0.90$ and 1.0. In view of the lack of a detailed theory about the formation of iron WDs, we have taken into account for each stellar mass different

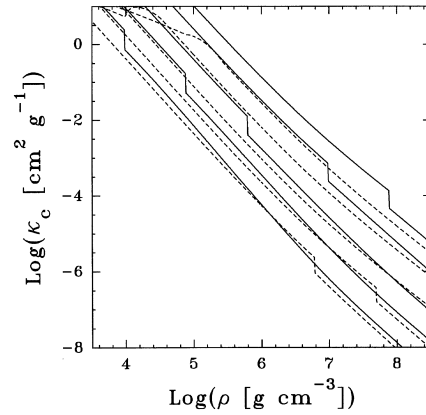


Figure 1. Conductive opacities for iron (solid line), and for 50 per cent carbon–50 per cent oxygen (short dashed lines) plasmas. Curves correspond, from bottom to top, to temperatures of 5×10^6 , 10^7 , 2×10^7 , 5×10^7 and 10^8 K, respectively. Note the steps in the curves that correspond to crystallization of the plasma.

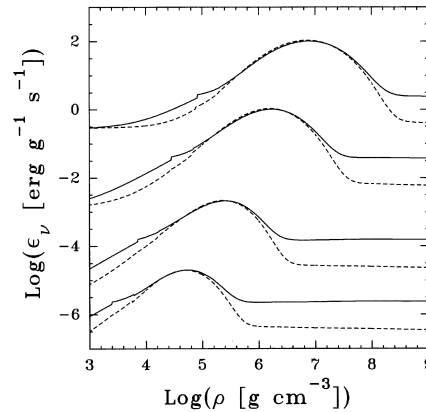


Figure 2. Neutrino energy loss rates for iron (solid line), and for 50 per cent carbon–50 per cent oxygen (short dashed lines) plasmas. Curves correspond from bottom to top to temperatures of 10^7 , 2×10^7 , 5×10^7 and 10^8 K, respectively. For a given temperature, at low densities, the dominant neutrino emission process is due to photo neutrinos. At higher densities a bump in the emission rate appears due to plasma neutrinos, whereas at highest densities, Bremsstrahlung neutrinos dominate.

chemical stratifications. Specifically, we have adopted pure iron cores embracing 99 (hereafter referred to as pure iron models), 75, 50 and 25 per cent of the total stellar mass plus (in the last three cases) a CO envelope. We have also examined the evolution of models with a homogeneous composition of iron and CO, by adopting a mass fraction for iron of 0.25, 0.50 and 0.75. In the interests of comparison, we have also computed the evolution of standard CO WD models. Because standard WDs of different stellar masses are expected to have different internal composition of CO, we have adopted the chemical profiles (kindly provided to us by I. Domínguez) resulting from recent evolutionary calculations of WD progenitors (Salaris et al. 1997). These profiles are also considered in the CO envelope of our iron models. In all the cases just described, we have taken into account the presence of an outer helium envelope with mass $M/M_* = 0.01$ and adopted a metallicity Z of 0.001. In the case of pure iron models, the transition from iron to helium layers is assumed to be almost discontinuous. We have also analysed the effect of a hydrogen envelope on iron models by including a pure hydrogen envelope

with $M/M_* = 10^{-5}$ on the top of the helium envelope (in this case we considered $Z = 0$). Models with and without a hydrogen envelope will be hereafter referred to as DA and non-DA, respectively. The main results of the present work are summarized in Figs 3–21. For completeness, we have extended our calculations to the cases of stellar mass of $0.4 M_\odot$, which most probably would have their origin in binary systems.

We begin by examining Fig. 3 in which we show the neutrino luminosity in terms of photon luminosity for pure iron and CO models. As expected, high-mass models fade away in neutrinos at higher luminosities than those corresponding to low-mass models. Such behaviour is found for both types of interior compositions considered here. However, because iron plasma is more efficient neutrino emitter than CO (see Fig. 2), note that for a given mass

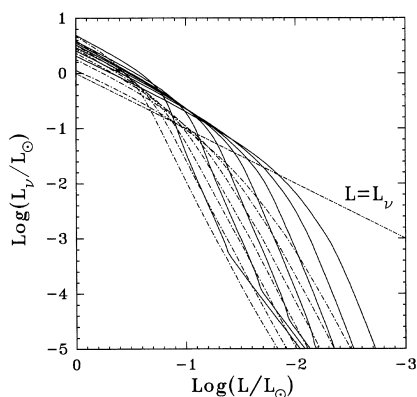


Figure 3. Neutrino luminosity versus photon luminosity corresponding to pure iron (full lines) and CO (dot–dashed lines) non-DA WD models with stellar masses $M/M_\odot = 0.40, 0.50, 0.60, 0.70, 0.80, 0.90$ and 1.0 . For the sake of reference, the line $L_\nu = L_\gamma$ is also shown. The higher the model mass, the faster the fading in neutrino luminosity. Clearly, iron WDs are much more efficient neutrino energy radiators. In fact, neutrino emission represents the main cooling agent for iron WDs up to luminosities significantly lower than those corresponding to the standard case of CO WDs.

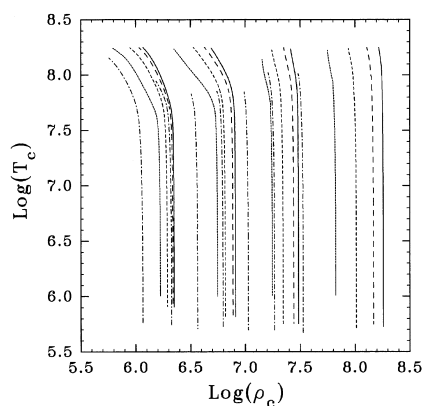


Figure 4. Central temperature versus central density for iron and CO non-DA models with masses of $M/M_\odot = 0.40, 0.60, 0.80$ and 1.0 (the higher the mass the higher the central density). For each stellar mass we depict the results corresponding to CO models (dot–dashed line), and to models with pure iron cores embracing 25, 50 and 75 per cent of the total stellar mass plus a CO envelope (dotted, short-dashed and long-dashed lines, respectively). Finally, full lines correspond to pure iron non-DA models. Notice that for a fixed mass value, iron-rich WDs have asymptotic central density values few times higher than the corresponding to CO WDs.

and photon luminosity, iron WDs have appreciably higher neutrino luminosity. Consequently, neutrinos are the dominant energy-release channel for iron WDs up to luminosities markedly lower than those corresponding to standard CO WDs.

The relation between central temperature and density for iron-rich

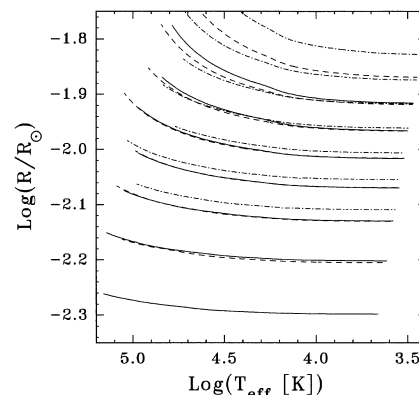


Figure 5. Radii in terms of effective temperature corresponding to pure iron (full lines) and CO (dot–dashed lines) non-DA models, and to models with a pure iron core containing half of the total stellar mass (dashed lines) for masses $M/M_\odot = 0.40, 0.50, 0.60, 0.70, 0.80, 0.90$ and 1.0 (the higher the mass the smaller the radius).

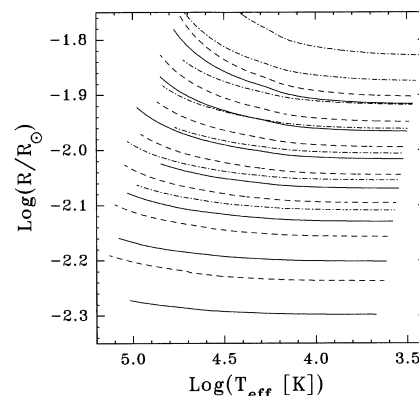


Figure 6. Same as Fig. 5, but now dashed lines show the results for homogeneous iron models with a iron abundance by mass of 0.5.

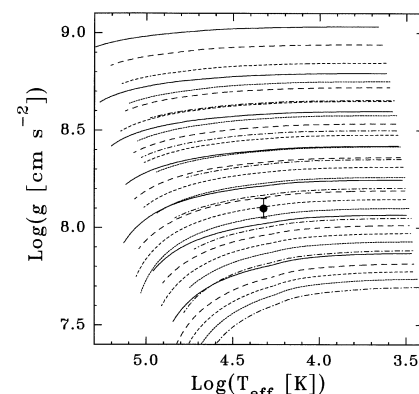


Figure 7. Surface gravities versus effective temperature relation corresponding to pure iron and CO non-DA models with masses of $M/M_\odot = 0.40, 0.50, 0.60, 0.70, 0.80, 0.90$ and 1.0 (the higher the mass the higher the surface gravity). The meaning of the lines is the same as in Fig. 4. The observational data corresponding to EG 50 are also included.

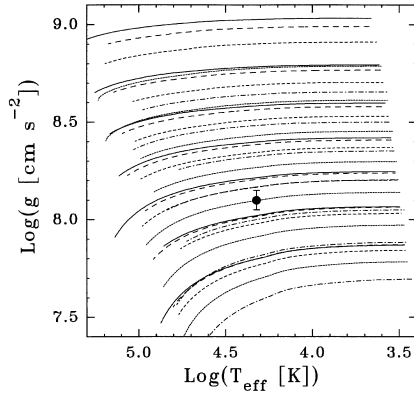


Figure 8. Same as Fig. 7 but for homogeneous iron models.

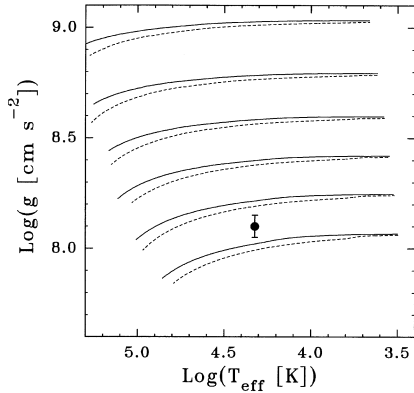


Figure 9. Surface gravity versus effective temperature relation corresponding to pure iron models of type non-DA and DA (solid and dotted lines, respectively) with masses of $M/M_{\odot} = 0.50, 0.60, 0.70, 0.80, 0.90$ and 1.0 (the higher the mass the higher the surface gravity). The inclusion of a hydrogen envelope leads to somewhat smaller gravity values. The observational data corresponding to EG 50 are also included.

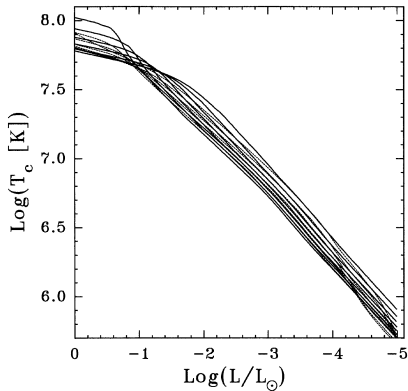


Figure 10. Central temperature as a function of photon luminosity corresponding to pure iron (full lines) and CO (dotted lines) non-DA models with masses of $M/M_{\odot} = 0.40, 0.50, 0.60, 0.70, 0.80, 0.90,$ and 1.0 . At low luminosities, the higher the mass the lower the central temperature.

and CO models is shown in Fig. 4. As we have considered models only in the WD regime, these curves are almost vertical straight lines, i.e. the density of the objects remained almost constant during the computed stages. As is well known, the higher the mass, the higher the central density of a WD, but note that for a fixed mass value, iron-rich WDs have central densities

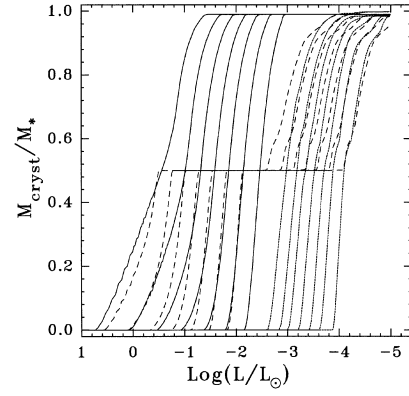


Figure 11. Evolution of the crystallization front in the Lagrangian coordinate as a function of luminosity corresponding to pure iron (full lines) and CO (dotted lines) non-DA models, and to models with a pure iron core containing half of the total stellar mass (dashed lines) for stellar masses of (from right to left) $M/M_{\odot} = 0.40, 0.50, 0.60, 0.70, 0.80, 0.90$ and 1.0 . Note that iron models crystallize at luminosities far higher than those corresponding to their CO counterparts. This is a result of the strong electrostatic coupling of the iron plasma. Note also that once the iron core is completely crystallized, crystallization conditions at the CO plasma are reached only at much later evolutionary stages.

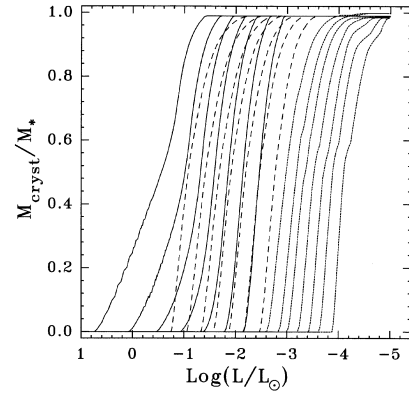


Figure 12. Same as Fig. 11, but now dashed lines show the results for homogeneous iron models with an iron abundance by mass of 0.5 .

appreciably higher than those corresponding to CO WDs. This is true even for models containing an iron core of only 25 per cent of the total mass. The higher densities are a result of basically two effects: one is the higher mean molecular weight-per-electron for iron plasma ($\mu_e = 2.151344$ for iron, whereas $\mu_e = 2.000000$ and 1.999364 for carbon and oxygen, respectively). The other effect is that, because of the high atomic number ($Z = 26$), iron plasma is subject to much stronger interactions than a CO one. Thus, for a given particle number density, as corrective terms of the pressure are negative, an iron plasma exerts less pressure, forcing a larger internal density than for CO WDs. It is worth mentioning that as the objects cool down, their internal temperature goes to zero. Thus, the global structure of the objects asymptotically tends to that predicted by Hamada & Salpeter (1961), as expected.¹

Another important characteristic of the models are their radii and surface gravities shown in Figs 5 to 9 as a function of effective temperature. Hot WD models have larger radii, owing mainly to the inflation of their non- and partially degenerate outer layers. It

¹For the sake of clarity, we do not include the results corresponding to the Hamada & Salpeter zero-temperature objects.

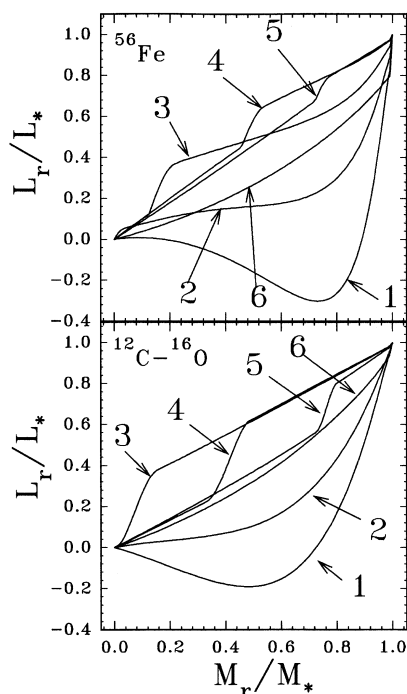


Figure 13. Profile of the relative luminosity versus the fractional mass for non-DA WDs models with $0.6 M_{\odot}$ having pure iron (upper panel) and CO (lower panel) interiors. For the case of the iron models we have included the profiles corresponding to luminosities of $\log L/L_{\odot} = -0.9004, -1.4154, -1.6554, -1.8588, -2.0301$ and -4.9643 labelled from 1 to 6 respectively; whereas for CO models the luminosities are $\log L/L_{\odot} = -0.67, -0.95, -3.49, -3.65, -4.00$ and -4.90 labelled from 1 to 6, respectively. For details, see text.

is quite noticeable that iron WDs have a much smaller (higher) radii (gravitational acceleration) than their CO counterparts. Note also that, for the same stellar mass and iron content, models with pure iron cores are clearly less compact than homogeneous iron models. These results can be compared with the observational data of Provencal et al. (1998) to infer the core chemical composition of their WD sample. In particular, we add in Figs 7 and 8 the observational data for the enigmatic case of EG 50, for which Provencal et al. (1998) quoted a surface gravity of $\log g = 8.10 \pm 0.05$, an effective temperature of $21\,700\text{ K} \pm 300\text{ K}$ and a stellar mass (derived without relying on a mass–radius relation) of $0.50 M_{\odot} \pm 0.02 M_{\odot}$. Having the stellar mass, we are in a position to estimate the core composition for this star. In this context, we find that these values are compatible with a pure iron model of $M \approx 0.52 M_{\odot}$. They are also consistent with homogeneous models with an iron abundance by mass greater than ≈ 0.75 . In Fig. 9 we show the effect of a thick hydrogen envelope on our pure iron models. The presence of such an envelope gives rise to somewhat smaller gravities, an opposite trend to what is needed to fit the current observations of EG 50. For completeness, we show in Fig. 10 the central temperature versus photon luminosity relation for some selected models. Note the change of slope at high luminosities, reflecting the end of the neutrino-dominated era.

As stated above, we have also considered crystallization in our models. We assumed that crystallization sets in when the plasma coupling constant Γ reaches the value $\Gamma_m = 180$, where

$$\Gamma = 2.275 \times 10^5 \frac{\rho^{1/3}}{T} \left(\frac{\langle Z \rangle}{\langle A \rangle} \right)^{1/3} \langle Z^5 \rangle^{1/3}, \quad (1)$$

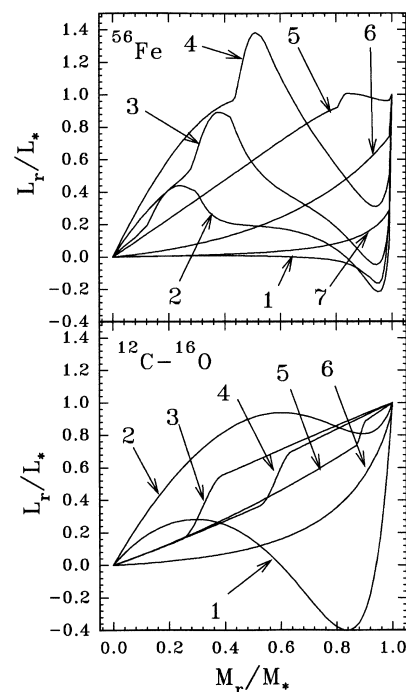


Figure 14. Profile of the relative luminosity versus the fractional mass for non-DA models with $1.0 M_{\odot}$ WDs having pure iron (upper panel) and CO (lower panel) interiors. For the case of the iron models we have included the profiles corresponding to luminosities of $\log L/L_{\odot} = 1.58447, 0.1668, -0.1771, -0.5043, -0.9652, -3.8293$ and -4.9036 labelled from 1 to 7 respectively; whereas for CO models the luminosities are $\log L/L_{\odot} = -0.12, -0.65, -2.86, -3.05, -3.44$ and -5.00 labelled from 1 to 6, respectively. For details, see text.

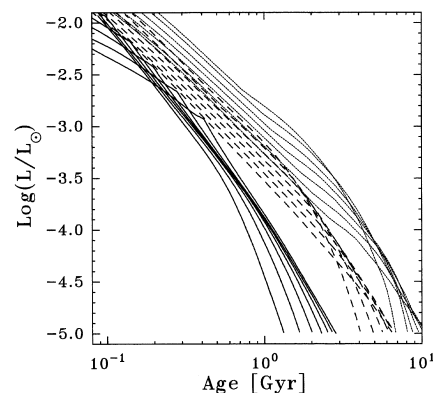


Figure 15. Age versus luminosity relation corresponding to pure iron (full lines) and CO (dotted lines) non-DA models, and to models with a pure iron core containing half of the total stellar mass (dashed lines) for stellar masses of $M/M_{\odot} = 0.40, 0.50, 0.60, 0.70, 0.80, 0.90$ and 1.0 . Note that pure iron models cool down about five times faster than standard CO WDs. At the high luminosities of this figure, the change in the slope of pure iron models is a result of the discontinuity of conductive opacity at the crystallization front. See text for details.

where $\langle A \rangle$ and $\langle Z \rangle$ denote, respectively, the averages over abundances by number of the atomic mass and charge of the different species of ions (see Segretain et al. 1994). Our choice of the Γ_m value is in accordance with studies carried out by Ogata & Ichimaru (1987) and Stringfellow, De Witt & Slattery (1990), and it has been used in recent WD evolutionary calculations such as Segretain et al. (1994) and Salaris et al. (1997).

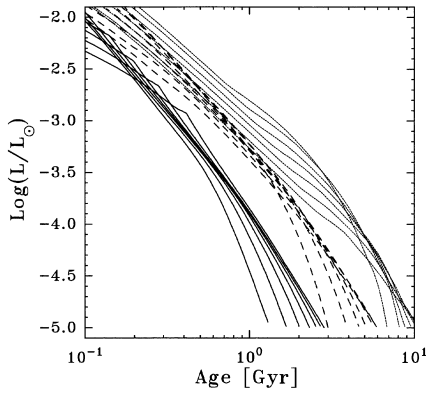


Figure 16. Same as Fig. 15, but now dashed lines show the results for homogeneous iron models with an iron abundance by mass of 0.5.

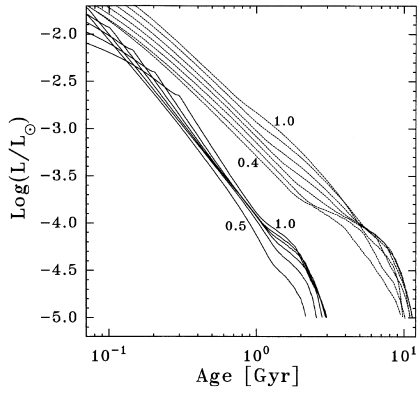


Figure 17. Age versus luminosity relation corresponding to pure iron (full lines) and CO (dotted lines) DA models for stellar masses of $M/M_{\odot} = 0.40, 0.50, 0.60, 0.70, 0.80, 0.90$ and 1.0 (for iron models the minimum mass value shown is $0.5 M_{\odot}$). Note that pure iron models cool down about five times faster than standard CO DA WDs. At the high luminosities of this figure, the change in the slope of pure iron models is a result of the discontinuity of conductive opacity at the crystallization front. See text for details.

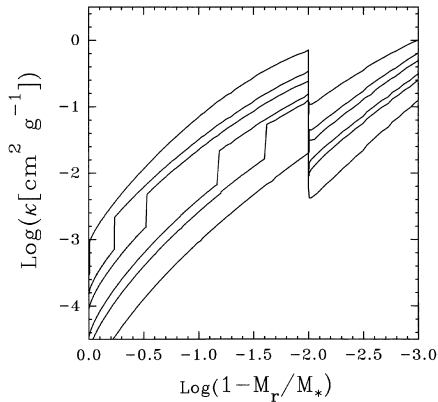


Figure 18. Opacity in terms of the outer mass fraction for pure iron DA models with $0.6 M/M_{\odot}$. From top to bottom, curves correspond to different evolutionary stages characterized by $\log L/L_{\odot} = -1.31, -1.78, -1.95, -2.23, -2.35$ and -2.71 . Note the change of iron opacity at the crystallization front. At $M_r/M_* = 0.99$, the change in the opacity is due to the presence of helium in the outer layers.

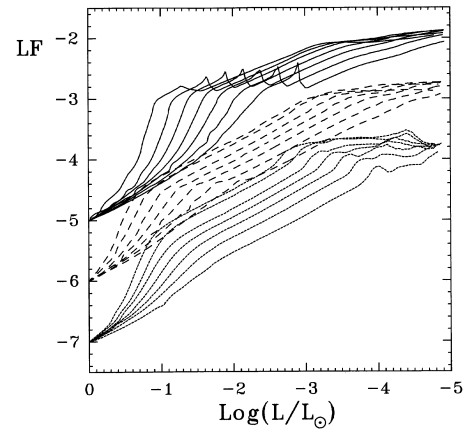


Figure 19. Single luminosity functions (normalized at $\log L/L_{\odot} = 0$) in terms of surface luminosity for pure iron (full lines) and CO (dotted lines) non-DA models, and to models with a pure iron core containing half of the total stellar mass (dashed lines) for stellar masses with (from bottom to top) $M/M_{\odot} = 0.40, 0.50, 0.60, 0.70, 0.80, 0.90$ and 1.0 . For the sake of clarity we have set arbitrarily $LF = -5, -6$ and -7 for the three set of curves. For the spikes in the iron LFs, see text.

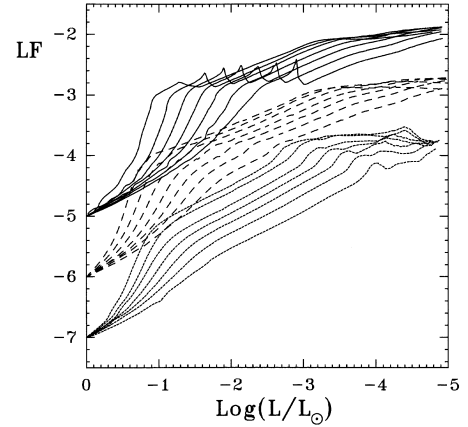


Figure 20. Same as Fig. 19, but now dashed lines show the results for homogeneous iron models with a iron abundance by mass of 0.5.

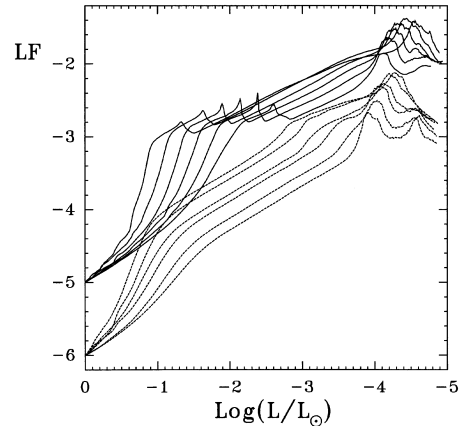


Figure 21. Single luminosity functions (normalized at $\log L/L_{\odot} = 0$) in terms of surface luminosity for pure iron (full lines) and CO (dotted lines) DA models for stellar masses with (from bottom to top) $M/M_{\odot} = 0.50, 0.60, 0.70, 0.80, 0.90$ and 1.0 . For the sake of clarity we have set arbitrarily $LF = -5$ and -6 for the two set of curves. For the spikes in the iron LFs, see text.

The growth of the crystal phase in our models is shown in Figs 11 and 12 as a function of photon luminosity. Very large differences are found between the crystallization of iron WDs compared with the case of standard CO WDs. If we assume a pure iron composition, then $Z_{\text{Fe}}^2/A_{\text{Fe}}^{1/3} = 176.69$, whereas considering pure carbon and oxygen $Z_{\text{C}}^2/A_{\text{C}}^{1/3} = 15.72$ and $Z_{\text{O}}^2/A_{\text{O}}^{1/3} = 25.39$, respectively. Thus, iron plasma reaches crystallization conditions much earlier during the evolution. In addition, the interior of iron WDs is much denser than in the standard case, as noted earlier. As a result, crystallization of iron WDs sets in at such high luminosities that neutrino emission is the main agent of energy release. This is in clear contrast to the case of CO WDs, which undergo crystallization at luminosities low enough that neutrino emission has already faded away. It should be noted that for $1.0 M_{\odot}$ and $0.40 M_{\odot}$ pure iron models, the onset of crystallization occurs at luminosities 2000 and 50 times higher than the corresponding CO WDs with the same mass. In the case of models with a pure iron core plus a CO envelope, Fig. 11 depicts an interesting feature worthy of comment. Indeed, the weaker electrostatic coupling of CO plasma as compared to iron plasma leads to a halt in the growth of the crystalline phase once the iron core has been completely crystallized. It is only at much later evolutionary stages that the crystallization process will set in again. It is worth mentioning that in the case of iron WDs, the analytic treatment of the growth of the crystal phase presented in Benvenuto & Althaus (1995) is no longer valid, simply because in that work it was assumed an isothermal interior.

As is well known, the crystallization of the interior of WDs has two effects on the evolution. One is the release of latent heat, which acts as an energy source that delays the evolution. The other is the change of the specific heat at constant volume C_v . In fact, ions are no longer free but subject to undergo small oscillations around its corresponding lattice equilibrium position. In such a case, $C_v = 3kD(\theta_D/T)$ where D is the Debye function and $\theta_D = 1.74 \times 10^3 (2Z/A)\rho^{1/2}$ is the Debye temperature. Eventually, at low-enough temperatures, $C_v \rightarrow (T/\theta_D)^3$. Thus, the crystallized interior has a lower ability to store heat, giving rise to an acceleration of the cooling process.

In order to get a deeper insight into the role of these effects in the evolution of iron WDs, we present in Figs 13 and 14 the profile of interior luminosity relative to its surface value at selected stages of the evolution of iron and CO WDs with $0.6 M_{\odot}$ and $1.0 M_{\odot}$ as a function of the fractional mass. Let us first discuss the results corresponding to the $0.6 M_{\odot}$ models (Fig. 13). In either of the iron and CO cases, curves labelled 1 correspond to an evolutionary stage at which neutrino luminosity dominates, giving rise, as is well known, to negative luminosity values. From then on, in the case of CO WDs (lower panel of Fig. 13), neutrinos fade away, producing a linear, smooth profile (corresponding to evolutionary stages limited by curves 2 and 3). Afterwards, the interior crystallizes, as is reflected by the change of slope in curves 3, 4 and 5. Such a change of slope is due to the release of latent heat. Note also the outwards direction of the propagation of the crystallization front as cooling proceeds.

Let us now discuss the results corresponding to the case of $0.6 M_{\odot}$ iron WD (upper panel of Fig. 13). As crystallization occurs very early, some of the evolutionary stages that we have selected correspond to high luminosities. The curve labelled as 1 reaches negative L values because of neutrino emission and curve 2 corresponds to a stage soon after the onset of crystallization. From then on, the crystal front moves outwards during the early stages of evolution. Note the large differences found in the

luminosity profile in this case as compared to the standard one, largely owing to the fact that much of the released latent heat is lost by neutrino emission.

In the case of $1.0 M_{\odot}$ models, the differences are dramatically enhanced (see Fig. 14). The CO model (lower panel) shows profiles very similar to the previous CO case with the exception of the last stage of evolution included, for which, as a result of the decrease in the specific heat C_v , the profile is no longer linear. In the case of the iron model, curve 1 corresponds to a stage previous to the onset of crystallization. Curves 2, 3, 4 and 5 represent stages at which the crystal front moves outwards. Over these evolutionary stages, latent heat is lost away by neutrino emission. Finally, curve 7 corresponds to a stage so advanced that most of the luminosity is provided by compression of the outermost layers. Indeed, most of the iron core has a very low luminosity because of its very low specific heat ($\theta_D/T \approx 40$).

Let us remind the reader that C_v is proportional to the number of particles. Thus, per gram of material, C_v is inversely proportional to the atomic weight of the constitutive isotopes. As a consequence, for a given stellar mass value, iron WDs have a lower total capacity of storing heat than that corresponding to the standard case in about (assuming a mixture of 50 per cent carbon and 50 per cent oxygen) $56/(0.5 \cdot 12 + 0.5 \cdot 16) = 4$. Thus, it is clear that iron WDs should cool faster than CO ones, as it is shown in Figs 15–17. In these figures we show the time spent by objects to cool down to a given luminosity (at the luminosity stages shown in the figures, our election for the zero-age point, $\log L/L_{\odot} = 0$, is immaterial). We find that in reaching a given luminosity value, low-luminosity pure iron models have to evolve in about a fifth of the time that a CO WD need! The abrupt change in the rate of cooling of pure iron models (as reflected by the change of slope in the age–luminosity relationship) at the high-luminosity range of these figures is worthy of comment. In fact, it occurs when the crystal front has just reached the outer layers of the iron core. Because of the discontinuity of iron conductivity opacity at the melting temperature (see Fig. 1), these layers become suddenly much more transparent. The opacity of these layers plays a significant role by regulating the heat flow from the interior to the outer space; thus, such a discontinuity in the opacity is expected to affect the rate of cooling. The situation is more clearly illustrated by Fig. 18 in which the behaviour of opacity (conductive plus radiative) is shown in terms of the outer mass fraction for a pure iron model with $M/M_{\odot} = 0.6$ at different evolutionary stages. Note that very deep in the star, conduction is very efficient, so the discontinuity in the opacity will play a minor role. It is only when crystallization reaches the very outer layers of the iron core that the cooling rate will be affected. This explains the fact that the induced effect on the cooling times is negligible for models having only half of their stellar masses composed of iron. The effect of a hydrogen envelope on cooling of pure iron models is depicted in Fig. 17. As expected, the presence of a hydrogen envelope increases the evolutionary times at very low luminosities. In part, this is due to the excess of thermal energy that the star has to get rid of when degeneracy reaches the base of the convection zone, thus producing a bump in the cooling curves (see D’Antona & Mazzitelli 1989 for a discussion in the context of CO WD models). We should mention that in the present calculations we have not investigated the effect of separation of carbon and oxygen during crystallization on the age of our CO models (see Salaris et al. 1997 and references therein); nor did we take into account the effect of iron–carbon phase separation analysed by Xu & Van Horn (1992). In view of the fact that iron-rich WDs

crystallize at high luminosities, we judge that the induced delay in the cooling times of our iron-rich models brought about by chemical redistribution at solidification would be of minor importance, although more details calculations would be required to place this assertion on a more quantitative basis.

Assuming a constant birthrate of WDs, we have computed single luminosity functions (LF) as $dt/d\log LL_{\odot}$ for our set of models. The results are displayed in Figs 19–21. For clarity we arbitrarily fixed the value of $dt/d\log L/L_{\odot} = -5, -6$ and -7 at $\log L/L_{\odot} = 0$ for the two sets of iron and CO composition respectively. As in the previous figures, the differences between iron and CO WDs are large. For iron objects at stages for which the crystalline phase is still growing, the slope of the LF is rather larger than for the CO case, especially for high-mass objects. A striking feature shown by these figures are the spikes characterizing the LFs of the pure iron sequences, which are directly understood in terms of the discussion presented in the foregoing paragraph. As explained, when the crystal front reaches the outer layers of the iron core, they become suddenly much more transparent (as a result of the discontinuity of conductive opacity at the melting temperature, see Fig. 18), giving rise to an abrupt change in the rate of cooling of models, which translates into a discontinuity in the derivative of the evolutionary times. Thus, LF shows a step downwards and then again increases steadily up to the lowest L considered here. We want to mention that the behaviour of our theoretical luminosity functions at the lowest luminosity values computed here may be affected by extrapolation of available opacity data.

4 DISCUSSION AND CONCLUSIONS

Motivated by recent observational evidence that seems to indicate the existence of white dwarf (WD) stars with iron-rich cores (Provencal et al. 1998), we have studied the evolution of iron-core WDs.

In this paper we have constructed detailed evolutionary sequences of WD stars with different chemical stratifications. Specifically, we have computed the evolution of models with masses of $M/M_{\odot} = 0.40, 0.50, 0.60, 0.70, 0.80, 0.90$ and 1.0 with pure iron cores embracing 99, 75, 50 and 25 per cent of the total stellar mass plus (in the last three cases) a CO envelope. We have also examined the evolution of models with a homogeneous composition of iron and CO, by adopting a mass fraction for iron of 0.25, 0.50 and 0.75. For comparison purposes with standard results we have also computed the evolution of CO WD models having the same masses. All of the models were assumed to have an outer helium envelope of $M/M_{*} = 0.01$, and in some cases we analysed the effects of the presence of a hydrogen envelope. In computing the structure of such objects we employed a detailed evolutionary code updated to account for the physics of iron plasmas properly.

In a set of figures we examined neutrino luminosities, central densities and temperatures, radii, surface gravities, crystallization, internal luminosity profiles, ages and the luminosity function (at constant birth rate). Our results indicate that iron WDs evolve in a very different way, as compared with standard CO WDs. These differences are due to the fact that the mean molecular weight per electron for iron is higher than for CO plasmas and also due to the stronger corrections to the ideal degenerate equation of state that causes the pressure of iron plasmas to be below the values corresponding to the case of CO.

As a consequence of the denser interior, iron WDs have smaller radii, greater surface gravities, higher internal densities, etc. compared with standard CO WDs of the same mass. We have compared the predictions of our models with the current observational data of the WD EG 50, for which Provencal et al. (1998) have suggested an iron-rich composition. In particular, we found that this object is consistent with WD models having a pure iron composition. Likewise, very noticeable are the differences encountered in the crystallization process that occurs at very high luminosities. For example, the onset of crystallization occurs, for the case of a $1 M_{\odot}$ pure iron model, at a luminosity 2000 times higher than the corresponding to the case of a CO object with the same stellar mass.

Because iron particles are much heavier than carbon or oxygen, the specific heat per gram is much lower, indicating that the interior of iron WDs is able to store comparatively small amounts of heat. Thus, it is not surprising that the cooling process at very low luminosities proceeds in a much faster way than the standard case.

We have also computed the single luminosity function for each computed sequence. It is nevertheless worth noticing that, owing to the uncertainties present in the birth process, we have not constructed an integrated luminosity function for the computed iron WD sequences. In any case it should be noticed that if pure iron WDs, to which class EG 50 seems to belong, were very numerous, some of them would have had time enough to evolve to luminosities much lower than the corresponding to the observed fall-off of the WD luminosity function ($\log L/L_{\odot} \approx -4.5$, see Leggett, Ruiz & Bergeron 1998 for details). Thus, from a statistical point of view, the lack of a tail in the observed luminosity function strongly indicates a low spatial density of pure iron WDs and may be employed to quantitatively constraint it.

Detailed tabulations of the results presented in this paper are available upon request to the authors at their email addresses.

ACKNOWLEDGMENTS

We are deeply acknowledged to our anonymous referee, whose suggestions and comments greatly improved the original version of this work. We are also grateful to I. Domínguez for sending us the chemical profiles of her pre-white dwarf models. OGB wishes to acknowledge Jan-Erik Solheim and the LOC of the 11th European Workshop on White Dwarfs held at Tromsø (Norway) for their generous support that allowed him to attend that meeting where he became aware of the observational results that motivated the present work.

REFERENCES

- Althaus L. G., Benvenuto O. G., 1997, *ApJ*, 477, 313
- Althaus L. G., Benvenuto O. G., 1998, *MNRAS*, 296, 206
- Benvenuto O. G., Althaus L. G., 1995, *Ap&SS*, 234, 11
- Benvenuto O. G., Althaus L. G., 1997, *MNRAS*, 288, 1004
- Chabrier G., 1993, *ApJ*, 414, 695
- Chandrasekhar S., 1939, *An Introduction to the Study of Stellar Structure*, University of Chicago Press
- D’Antona F., Mazzitelli I., 1989, *ApJ*, 347, 934
- Hamada T., Salpeter E. E., 1961, *ApJ*, 134, 683
- Isern J., Canal R., Labay J., 1991, *ApJ*, 372, L83
- Itoh N., Hayashi H., Kohyama Y., 1993, *ApJ*, 418, 405
- Itoh N., Kohyama Y., Matsumoto N., Seki M., 1984a, *ApJ*, 285, 758

- Itoh N., Kohyama Y., Matsumoto N., Seki M., 1984b, *ApJ*, 285, 304
(erratum: 1987, *ApJ*, 322, 584)
- Leggett S. K., Ruiz M. T., Bergeron P., 1998, *ApJ*, 497, 294
- Ogata S., Ichimaru S., 1987, *Phys. Rev. A*, 36, 5451
- Provencal J. L., Shipman H. L., Hog E., Thejll P., 1998, *ApJ*, 494, 759
- Salaris M., Domínguez I., García-Berro E., Hernanz M., Isern J., Mochkovitch R., 1997, *ApJ*, 486, 413
- Saumon D., Chabrier G., Van Horn H. M., 1995, *ApJS*, 99, 713
- Savedoff M. P., Van Horn H. M., Vila S. C., 1969, *ApJ*, 155, 221
- Segretain L., Chabrier G., Hernanz M., García-Berro E., Isern J., Mochkovitch R., 1994, *ApJ*, 434, 641
- Stringfellow G. S., De Witt H. E., Slattery W. I., 1990, *Phys. Rev. A*, 41, 1105
- Xu Z. M., Van Horn H. M., 1992, *ApJ*, 387, 662

This paper has been typeset from a \TeX/L\TeX file prepared by the author.